Preprint
UCRL-JC-149940-REV-2

# A Comparison of the Effect of Temperature on the Passivity Breakdown and Repassivation Potentials of Wrought and Welded Alloy 22 in 5 M $CaCl_2$

*G. O. Ilevbare*

This article was submitted to *204th Meeting of the Electrochemical Society, Orlando, Florida*
*October 12-16, 2003*

U.S. Department of Energy
Lawrence Livermore National Laboratory

**August 11, 2003**

# A COMPARISON OF THE EFFECT OF TEMPERATURE ON THE PASSIVITY BREAKDOWN AND REPASSIVATION POTENTIALS OF WROUGHT AND WELDED ALLOY 22 IN 5 M $CaCl_2$

G. O. Ilevbare
Lawrence Livermore National Laboratory
7000 East Ave, L-631, Livermore CA 94550, USA

## ABSTRACT

The study of the electrochemical behavior of wrought and welded Alloy 22 was carried out in 5 M $CaCl_2$ between 45 and 120 °C. Comparisons were made between the electrochemical behaviors of the wrought and welded forms of Alloy 22 Multiple Crevice Assembly (MCA) specimens. The susceptibility to corrosion was found to increase with increase in temperature in both the wrought and the welded forms of the alloy. The weld metal was found to be less susceptible to localized corrosion under the conditions tested.

## INTRODUCTION

Alloy 22 (UNS number N06022) is a nickel alloy rich in chromium and molybdenum, with a high degree of corrosion resistance. It exhibits a low general corrosion rate under most conditions and has formidable localized corrosion resistance in most environments compared with other nickel alloys [1-8]. Alloy 22 is the candidate material for the fabrication of high-level nuclear waste containers. These containers are intended for use for disposal of high-level radioactive waste and spent nuclear fuel. On July 23, 2002, The United States Congress approved the site at Yucca Mountain, Nevada, for development as a repository for disposal of nuclear waste.

Since welding will be used to close the waste containers, it is important to fully characterize and understand the electrochemical behavior of the welds and the areas adjoining the welds. One method of comparison is to characterize the behavior of non-welded (wrought) and welded Alloy 22 to determine whether there is increased susceptibility to corrosion in the welded zones and areas adjacent to the welded zones.

The study of the effect of temperature on the corrosion properties of the alloy is important since during the projected 10,000-year service life, the containers will pass through a heat gradient caused by the heat generated from radioactive decay. Temperatures will be high (above the boiling point of water) in the early service life of the containers, while lower temperatures will prevail much later due to decreased radioactive decay. At this later stage, there is an increased possibility of ground water contacting the containers.

A range of water chemistries is expected to be in contact with the waste containers during its service live. The effect of important individual anions (like $Cl^-$), which could impact the performance of the containers, must be understood. Crevice corrosion is a concern in $Cl^-$ environments [2-4]. Consequently, the study of the crevice corrosion behavior of Alloy 22 in the wrought and welded forms has been carried out in 5 M $CaCl_2$ using a multiple crevice assembly (MCA) sample configuration. This configuration was optimized for the study of crevice corrosion as it provides 24 potential crevice generation sites on a surface area of less than 10 $cm^2$. The temperature range of study was between 45 and 120 °C (±2 °C).

## EXPERIMENTAL PROCEDURE

The material used in this study is Alloy 22 (N06022). Alloy 22 samples were fabricated from wrought and welded plate specimens. The chemical composition as documented by the supplier appears in Table 1. The composition is consistent with ASTM-B 575 (for plates/sheets) standard [9, 10]. The wrought samples were made out of flat sheets that were ~2 mm thick, while the welded samples were made from plates what were 3.175 cm (1.25 inch) thick. The composition of the filler metal was taken before it was used in the welding process. The Multiple Crevice Assembly (MCA) specimens look like lollipops (Figure 1). The design was optimized for the study of crevice corrosion so that most of the working surface was covered by the ceramic crevice former. The working surfaces of the MCA samples were used in the as-received state after degreasing with acetone and methanol. In the as-received state, the working surfaces of the MCA samples were finished to a root mean square (RMS) roughness average (RA) of between 2 and 5 micro inches with an air formed oxide film. The edge (surface 90 degrees in angle to the working surface) of the samples was finished with 600-grit SiC paper after first grinding with 100 and then 240-grit paper to remove damage done to them by the electric discharge machine (EDM) used during fabrication. The welded MCA specimens were identical to the wrought specimens in configuration. The welds were made by means of Gas Tungsten Arc Welding (GTAW). The double-U shaped welds were completed in about 8-10 passes (Figure 2). The weld metal on the welded samples was taken from the outermost portion (surface) of the welds. Since the welds had a double-U configuration, this meant that the volume of weld metal on the sample was not the same throughout the ~2 mm thickness of the samples. Nonetheless, the amount of weld metal on the samples covered an area on the working surface that was at least 1 cm wide and extended across the entire face (perpendicular to the stem of the sample) of the specimen on which the crevice formers were assembled. The rest of the MCA consisted of Titanium (Ti) grade 2 nuts, bolts and washers, as well as ceramic crevice formers with multiple ridges. The bolts were polytetrafluoroethylene (PTFE) wrapped to prevent these hardware components from being in electrical contact with the specimen. Each crevice former had a total of 12 ridges on it, creating 12 different potential crevice sites on each face of the specimen, and a total of 24 potential sites in each assembly (Figure 1). The assembly was tightened to a torque of 70 in-lb. PTFE tape inserts were placed between the ceramic crevice former and the MCA sample prior to tightening. This was done to fill in the micro voids created by the micro-rough surfaces of the sample and the ceramic crevice former, and to increase the reproducibly of the tight crevices in all samples. The total surface area of the MCA specimen

immersed in the electrolyte was 7.43 $cm^2$. This surface area included the area under the 24 ridges of the crevice formers, which had a combined surface area of 1.6 $cm^2$. In current density estimations, the surface area of 7.43 $cm^2$ was used for calculations.

A three-electrode cell with a capacity of 1000 $cm^3$ was used for experimentation. The volume of electrolyte in the cell was ~900 $cm^3$. A saturated silver/silver chloride (SSC) (Ag/AgCl) electrode was the reference electrode (RE). The RE was maintained near room temperature by mounting it at the end of a Luggin probe, which had a water-cooled jacket around it. The temperature of the water pumped through the cooling jacket was between 5 and 12 °C. Thermal liquid junction calculations showed that potential variation caused by this phenomenon was in the order of a few mV (~10 mV maximum). Also, according to Macdonald et al., a high KCl concentration in the reference electrode tends to suppress thermal liquid junction potentials across the boundary between the high and low temperature solutions [11]. The liquid junction potential variations were therefore ignored in further analyses. The counter electrode was made of platinum (Pt) foil. The temperature of the electrolyte was maintained by means of an oil-filled heating bath. The sample was immersed into the cell after the electrolyte had attained the desired temperature. This was done immediately after the grinding process. The temperature was taken before and after the experiment with a thermocouple immersed into the electrolyte. Electrochemical measurements were carried out using a potentiostat. The corrosion potential ($E_{corr}$) was monitored for 24 hours. This was followed by cyclic potentiodynamic polarization measurements immediately afterwards. Cyclic polarization was started approximately 100 mV below $E_{corr}$, and continued until the current density from the sample reached a maximum of up to 30 $mAcm^{-2}$, or a maximum of 1.3 V (SSC) before the scan was reversed. An upper limit of 30 $mAcm^{-2}$ was chosen to facilitate the observation of any anodic peaks that might occur (and repassivate) with current densities as high as 20-30 $mAcm^{-2}$ generated (especially at 75 °C) on Alloy 22 in 5 M $CaCl_2$. The sweep rate in the forward and reverse directions was 0.1667 $mVs^{-1}$ (600 $mVh^{-1}$). Deaerated 5 M $CaCl_2$ with a pH~5 was used, at various temperatures in these experiments. Nitrogen gas ($N_2$) was bubbled through the electrolytes for at least one hour before and throughout the experiments at a rate of ~100 cc per minute. All electrolytes were prepared using certified American Chemical Society (ACS) reagent grade chemicals. In other experiments, potentiostatic polarization experiments were carried out for up to 24 hours in the same three-electrode configuration cell immediately after the 24-hour corrosion potential ($E_{corr}$) monitoring period.

## EXPERIMENTAL RESULTS

### The Corrosion Potential ($E_{corr}$)

Figure 3 shows a summary of the average $E_{corr}$ values between 45 °C and 120 °C for wrought and welded samples of Alloy 22. The number of repeats which make the average values presented range from 3 to 6. The error bars in Figure 3 are the standard deviations of the distributions. In each experiment, $E_{corr}$ was recorded at the end of the 24-hour period of the experiments, and used to compute the averages shown. Figure 3 shows that $E_{corr}$ from the wrought and welded specimens can only be separated with

confidence at 45 and 90 °C. They are statistically similar at all other temperatures as indicated by the overlapping of the error bars. The $E_{corr}$ of the wrought samples was not affected by temperature. The difference between the highest and lowest mean values of $E_{corr}$ between 45 and 120 °C was ~20 mV. However, the welded samples were affected by temperature. The $E_{corr}$ of welded samples decreased with increase in temperature. There was a difference of ~120 mV between the highest and lowest mean $E_{corr}$ values recorded on the welded samples. Nonetheless, the $E_{corr}$ values for the wrought and welded metals were relatively close over the entire range of temperature considered in these measurements (Figure 3).

The Breakdown Potential ($E_{crit}$)

The critical breakdown potential, $E_{crit}$, as employed here is used to denote the potential(s) at which the breakdown of the passive film occurs by any type of corrosion attack such as pitting corrosion, crevice corrosion, general dissolution, or transpassive dissolution.

Figures 4 and 5 show representative polarization curves at the extremes of the temperature range tested (45 and 120 °C) for the wrought and welded MCA samples. At 45 °C, the curves for both the wrought and the welded forms of Alloy 22 showed a similar behavior, and overlap almost exactly. Localized breakdown due to crevice corrosion did not occur on any of the samples tested at this temperature on both the wrought and the welded samples. At 120 °C (Figure 5), the polarization curves of wrought and welded Alloy 22 are also similar. However, the welded sample exhibited a higher breakdown potential compared with the wrought sample. The polarization curves of the wrought at 60, 75 and 90 °C were similar to those collected from the welded samples at the corresponding temperatures. The polarization curves at 90 °C were similar to those at 120 °C. At 60 and 75 °C however, the shape of the curves, and thus the electrochemical behavior of Alloy 22 differ from those at 90 and 120 °C (Figure 6). In Figure 6, there is a drop in current density after an initial rise in current density from the passive region at 60 and 75 °C. This drop in current density created an "anodic peak" or "hump" usually between 0.0 and 0.5 $V_{SSC}$, however, broader peaks have occurred on samples at 75 °C. The peaks at 75 °C are broader and have higher peak current densities than those at 60 °C. These current excursions could sometimes reach values of about 20-30 $mAcm^{-2}$ at 75°C. After the anodic peak or hump, there is a secondary passive region. The current density of the secondary passive region was higher than that of the primary passive region. The current density of the secondary passive region at 75 °C was much than at 60°C. Beyond the secondary passive region, transpassive dissolution results on further increase of the applied potential. Localized corrosion was observed on samples (at 60 °C) where the potential was reversed at or near the peak current density in the anodic peak after inspection with an optical microscope. At 60 and 75 °C where the experiments proceeded to potentials corresponding to regions of transpassive dissolution, two types of damage were observed on the sample, localized corrosion, which occurred at potentials corresponding to the anodic peak or hump, and general dissolution due to transpassivation, which occurred at much higher potentials. As observed in Figure 6, no hystereses loop occurs (at 60 nor 75 °C) when the potential is taken to the transpassive region. Samples where the applied potential was reversed in the anodic peak did not exhibit any generalized dissolution. Not all the wrought samples tested at 60 °C (and none of the 3 welded samples tested at 60 °C) exhibited the hump. Only transpassive

dissolution occurred at higher potentials at 60 and 75 °C, consistent with the absence of hystereses loops at these elevated potentials. The reason for this behavior is not fully understood.

Figure 7 shows a summary of the breakdown potentials ($E_{crit}$) and the repassivation potential $E_{rp}$ for both the wrought and the welded samples. These data points are from an average of at least 2 data values. The error bars are standard deviations of the distribution. $E_{corr}$ values have been included for easy comparison with $E_{crit}$ and $E_{rp}$. The method used to determine $E_{crit}$ was the current density inflection (of the curve) method. In this method, $E_{crit}$ was the potential at which a permanent rise in current density from the passive region commenced. In most case, $E_{crit}$ was easily determined due to the abrupt increase in current indicative of the onset of localized breakdown (Figure 5). At 60 and 75 °C where anodic peaks or "humps" occur, $E_{crit}$ was taken as the base of the "hump". Samples held at a potential (~0.325 $V_{SSC}$) corresponding to the peak current density in the hump at 75 °C (Figure 6) in potentiostatic polarization experiments for up to 24 hours showed that the samples did not passivate. In fact, there was massive dissolution of the metal, hence the potential at base, where the current density started to rise was taken as $E_{crit}$. Figure 8 shows about 70,000 s of the current and current density transients from a potentiostatic experiment performed at 75 °C. The abrupt full in current and current density at about 67 000s possibly coincides with the detachment of the lollipop head from the stem of the sample (refer to Figure 1).

$E_{crit}$ decreases steadily with increase in temperature between 45 and 120 °C (Figure 7). At 45 °C, on both the wrought and the welded samples, $E_{crit}$ is due to transpassive dissolution and not localized breakdown. This is also true at 60 °C on the welded samples. At 75 °C and above, $E_{crit}$ represents localized breakdown on both the wrought and welded samples. $E_{crit}$ at 75 and 90 °C are difficult to separate statistically since the error bars overlap. However, at 120 °C, $E_{crit}$ is higher on the welded samples, and hence more resistant to localized corrosion compared with the wrought samples.

The degree of damage due to localized corrosion increased with increase in temperature. The crevices formed at 60 °C were the shallowest, and caused the least damage per unit area. Crevice corrosion hardly occurred in the weld metal zone in welded samples (Figures 9 and 10). Where they occurred, they were less severe than the crevices in the base metal zone. In Figure 9 (75 °C; 5 M $CaCl_2$), the band of weld metal appears darker than the base metal zone in the top portion of the photo. The deepest crevices are located in the base metal zone. Similarly, in Figure 10 (120 °C, 5 M $CaCl_2$), the deep crevices that formed in the lower base metal half of the image seem to terminate at the boundary of the base and weld metal. In Figure 10, the weld metal zone seems to deflect the growth path of the crevices away from itself, thus confining it to the base metal zone. These images suggest that the weld metal is significantly better able to resist localized attack in 5 M $CaCl_2$ in spite of the similarities in the $E_{crit}$ of the wrought and welded samples especially at 75 and 90 °C.

The Repassivation Potential ($E_{rp}$)

Two methods were used to measure the repassivation potential for localized corrosion, $E_{rp}$. In the first method, the repassivation potential was taken as the potential that

coincided with a current density of 1 $\mu Acm^{-2}$ ($1 \times 10^{-6}$ $Acm^{-2}$) on the reverse sweep of the cyclic polarization curves. "$E_{rp1}$" in Figure 7 denotes the values obtained in this fashion. In the second method, denote by "$E_{rp2}$" (Figure 7), the repassivation potential is the potential that coincided with the point at which the reverse and forward sweeps of the polarization curve intersected. Figure 7 shows that comparable values of $E_{rp}$ are obtained from the two methods, as exemplified in the similarities of $E_{rp1}$ and $E_{rp2}$. In fact, at 75, 90 and 120 °C, the values are statistically indistinguishable because of the overlap of the error bars. There are no $E_{rp}$ values for the wrought and welded samples at 45 °C, and for the welded samples at 60 °C since there was no localized corrosion on the samples at these temperatures. Although localized corrosion was observed on the wrought samples at 60 °C, and on both the wrought and welded samples at 75 °C, the $E_{rp}$ values assigned to Alloy 22 at these temperatures might not be the true $E_{rp}$ values. The reason for this that the damage sustained by these samples under the said conditions at the time of applied potential reversal was not localized corrosion, but rather transpassive dissolution (Figure 6). More accurate $E_{rp}$ values would be obtained by reversing the potential in the region where localized corrosion is active, that is, by the peak current density in the "hump". There is a difference of at least 240 $mV_{SSC}$ between $E_{crit}$ and $E_{rp}$ in the wrought and the welded samples, with $E_{rp}$ being lower potential as expected. $E_{rp}$ decreased with increase in temperature, just as $E_{crit}$ did. The $E_{rp}$ values are similar for both the wrought and the welded samples, even at 120 °C where $E_{crit}$ is different. All $E_{rp}$ values were higher than the corresponding $E_{corr}$ values (Figure 7). That is, to attain localized corrosion, of Alloy 22 in pure 5 M $CaCl_2$ solution, polarization above $E_{corr}$ is needed.

## DISCUSSION

A range of water compositions is expected to contact the waste containers at Yucca Mountain [12]. Understanding the effect of $Cl^-$ on the corrosion process is important for evaluating these environments. Hence, high $Cl^-$ only environments (5 M $CaCl_2$ (10 M $Cl^-$)) were evaluated in this study. It should be noted that waters sampled at from Yucca Mountain contain an array of anions and oxyanions, which include $NO_3^-$ and $SO_4^{2-}$, which have been found to inhibit localized corrosion in stainless steels and nickel alloys [13-22]. Indeed, earlier work showed that Alloy 22 is not susceptible to localized corrosion in simulated concentrated multi-ionic solutions [1].

The similarity in the values of the $E_{corr}$ (except at 45 and 90 °C) for the wrought and the welded samples over the temperature range tested suggest that there might be difficulty in creating and sustaining viable galvanic couples which could lead to localized breakdown of the oxide film either on the base metal or weld (depending on which potential is higher). A possible reason for this is because the composition for the weld metal in the welded sample is similar to that of the base metal (Table 1).

A limitation of the method used in the determination of $E_{crit}$ is that it is not able to give the exact potential at which localized breakdown commences. This is because the current values being monitored for localized corrosion is a composite of the passive current density and that due to localized corrosion. Therefore, in order for a current rise (over and above the passive (background) current) to be observed, the localized corrosion event would need to grow to such as size that would enable it to put out a current higher than

that of the passive current of the specimen. The amount of growth that is required would depend on how large the surface of the specimen is since it scales directly with the value of the background current. Generally, the smaller the sample, the earlier the current due to localized breakdown will be detected, and the closer the determined $E_{crit}$ will be to the actual potential at which localized breakdown commenced [23]. However, increasingly smaller samples might lead to elevated $E_{crit}$ values, as the number of potential sites for the nucleation of localized events reduces with size. Other methods like the current threshold method, in which a current or current density is used to determine the onset of localized corrosion is also froth with uncertainties with regard to determining the exact onset of localized corrosion. Too low a threshold current value will lead to $E_{crit}$ values in the regions where the sample is still passive. Too high a threshold value leads to $E_{crit}$ values that are too high. Hence, the current threshold method is best employed only as a basis for comparison amongst systems.

The similar values of $E_{crit}$ obtained at 75 and 90 °C, and higher values obtained at 120 °C for the wrought and welded samples of Alloy 22 in 5 M $CaCl_2$ suggest that in this environment, GTAW welds did not cause any adverse effect on the resistance of Alloy 22 to localized corrosion under the present test conditions. The images in Figure 9 and 10 suggest that the weld and base metal exhibit different propensities to crevice corrosion, with the weld metal able to better resist crevice corrosion. Since the welded samples do not contain pure weld metal, the values of $E_{crit}$ presented for both the welded and wrought samples might therefore reflect the $E_{crit}$ of the wrought or base metal, rather than that of the weld metal alone. Since the closeness of the $E_{corr}$ values between the wrought and the welded samples suggest that powerful galvanic couples may not be viable, or easy to sustain, the greater susceptibility of the base compared with the weld metal is believed to be due to a metallurgical effect. However, the fact that both weld and base metal are present on the same sample creates a difficulty in accurately acquiring the contribution of each metal type to the $E_{corr}$ of the welded MCA samples. Nonetheless, although the $E_{corr}$ of the welded sample is a composite of the $E_{corr}$ of the weld and base metals, the propinquity of the $E_{corr}$ of the wrought and welded samples strongly suggests that the $E_{corr}$ of pure base metal (wrought) might be close to that of pure weld metal. Clearly, more work is required in this area to understand, and possibly isolate the main reason(s) for the differences in susceptibility to localized corrosion.

The anodic peaks or "humps" exhibited by both the wrought and the welded versions of the sample at 60, and 75 °C are associated with localized attack that passivated upon increase in potential. In addition, there is some difficulty in reactivating the sites of localized breakdown after passivation has occurred. The reason why passivation took place after initial breakdown is not fully understood. However, potentiostatic polarization experiments carried out at potentials equivalent to the maximum current density in the anodic peak show that high current densities required to sustain metal dissolution are sustained (Figure 8).

## CONCLUSIONS

1. After 24 hours of exposure to 5 M $CaCl_2$, the $E_{corr}$ of the wrought MCA Alloy 22 is not affected by temperature between 45 and 120°C. However, after 24

hours of exposure to 5 M $CaCl_2$, the $E_{corr}$ of the welded MCA samples of Alloy 22 decreases ~120mV with increase in temperature between 45 and 120 °C.

2. During anodic potentiodynamic polarization, localized corrosion was observed on wrought samples of at 60 °C and above, and at 75 °C and above for the welded samples in 5 M $CaCl_2$. No localized corrosion was observed at 45 °C on both the wrought and welded samples, and at 60 °C on the welded samples in 5 M $CaCl_2$.
3. $E_{crit}$ shifted to lower potentials as temperature increased on both the wrought and welded samples in 5 M $CaCl_2$.
4. $E_{crit}$ was similar on the wrought and welded samples at 75 and 90°C but was lower on the wrought samples at 120 °C in 5 M $CaCl_2$.
5. The weld metal was found to be less susceptible to crevice attack compared with the base metal in the welded samples in 5 M $CaCl_2$.
6. Where localized corrosion occurred, the $E_{rp}$ was similar on both the wrought and the welded samples in 5 M $CaCl_2$.
7. $E_{rp}$ decreased with increase in temperature on the wrought and welded samples in 5 M $CaCl_2$.

## REFERENCES


1. G.O. Ilevbare T. Lian and J.C. Farmer, Environmental Considerations in the Studies of Corrosion Resistant Alloys for High-Level Radioactive Waste Containment Paper No. 02539, Corrosion 2002.
2. G.O. Ilevbare, Electrochemical Behavior of Alloy 22 in 5 M $CaCl_2$, Transportation Storage, and Disposal of Radioactive Materials, PVP-Vol. 449, p.55 2002. American Society of Mechanical Engineers (ASME), New York, USA.
3. B. A. Kehler, G.O. Ilevbare and J.R. Scully Corrosion, 57, pp. 1042, 2001.
4. B. A. Kehler, G. O. Ilevbare and J. R. Scully Corrosion 2001, Crevice Corrosion Behavior, of Ni-Cr-Mo Alloys: Comparison of Alloys 625 and 22, NACE Topical Research Symposium, p.30, March 2001.
5. Haynes International, Inc., Product Brochure H-2019E, Haynes International Inc. Kokomo, IN, p.22, 1997.
6. J. C. Farmer, D. McCright, G.E. Gdowski, F. Fang, T. Summers, P. Bedrossian, J. Horn, T. Lian, J. Estill, A. Lingenfelter, and W. Halsey, General and Localized Corrosion of Outer Barrier of High-Level Waste Container in Yucca Mountain, May 2000. Preprint UCRL-JC-138890, Lawrence Livermore National Laboratory, Technical Information Department Digital Library.
7. K.A. Gruss, G.A. Cragnolino, D.S. Dunn and N.Sridhar, Corrosion '98, Paper No. 149, 1998.
8. S.J. Lukezich, The Corrosion Behavior of Ni-Base High Performance Alloys in Simulated Repository Environments, MS Thesis, The Ohio State University 1989.
9. ASTM B574, Annual Book of ASTM Standards, Nonferrous Metal Products, Volume 02.04, p.531, American Society of Testing and Materials, West Conshohocken, PA (2000).

10. ASTM B575, Annual Book of ASTM Standards, Nonferrous Metal Products, Volume 02.04, p.535, American Society of Testing and Materials, West Conshohocken, PA (2000).
11. D.D. Macdonald, A.C. Scott, and P. Wentrcek, J. Electrochem. Soc., **126**, 908 (1978).
12. N.D. Rosenberg, G.E. Gdowski, and K.G. Knauss, Applied Geochemistry, 2001. **16**: p.1231.
13. R.C. Newman and T. Shahrabi, Corrosion Science, 1987. **27**: p.827.
14. H. Yashiro and K. Tanno, Corrosion Science, 1990. **31**: p. 485.
15. H.H Uhlig and J.R. Gilman, Corrosion, **20**, 289t (1964).
16. H. P. Leckie and H.H. Uhlig, J. Electrochem. Soc., **117**, 1152 (1966).
17. I.L. Rozenfeld, and I.S Danilov, Corrosion Science, **7**, 129 (1967).
18. E.A. Lizlovs and A.P. Bond, J. Electrochem Soc., **116**, 574 (1969).
19. Z. Szklarska-Smialowska, Corrosion Science, **11**, 209 (1971).
20. Z. Ahmed, Corrosion, **33**, 161 (1977).
21. H.H. Strehblow, and B. Titze, Corrosion Science, **17**, 461 (1977).
22. H.C. Man and D. R. Gabe, Corrosion Science, **21**, 713 (1981).
23. G.T Burstein and G. O. Ilevbare, in Corrosion Science, **38**, 2257 (1996).

## Acknowledgements

The Department of Energy Office of Civilian Radioactive Waste Management (OCRWM) sponsored this work. This work was done under the auspices of the U.S. Department of Energy (DOE) by the University of California, Lawrence Livermore National Laboratory (LLNL) under contract No. W-7405-Eng-48. This work is supported by the DOE Office of Repository Development, LLNL.

Table 1. Chemical composition of Alloy 22 (UNS No. N06022) given in weight percent.

| Element | Actual Composition | | | ASTM Requirements ASTM B575-Sheets |
|---|---|---|---|---|
| | Wrought | Welded (Weld/Filler Metal) | Welded (Base Metal) | |
| **Mo** | 14.10 | 14.00 | 13.82 | 12.5-14.5 |
| **Cr** | 22.00 | 20.54 | 20.38 | 20.0-22.5 |
| **Fe** | 4.50 | 2.08 | 2.85 | 2.0-6.0 |
| **W** | 2.70 | 3.10 | 2.64 | 2.5-3.5 |
| **Co** | 1.30 | 0.03 | 0.01 | 0.0-2.5 |
| **C** | 0.003 | 0.004 | 0.005 | 0.000-0.015 |
| **Si** | 0.03 | 0.06 | 0.05 | 0.00-0.08 |
| **Mn** | 0.31 | 0.20 | 0.16 | 0.00-0.50 |
| **V** | 0.16 | 0.03 | 0.171 | 0.00-0.35 |
| **P** | 0.01 | 0.004 | 0.008 | 0.00-0.02 |
| **S** | <0.01 | 0.001 | 0.0002 | 0.00-0.02 |
| **Ni** | Bal. | Bal. | Bal | Bal. |

Wrought Specimens from Heat # 2277-5-3203. Welded Specimens: Base metal from Heat #059902LL1; Weld/filler metal from Heat # XX1753BG.

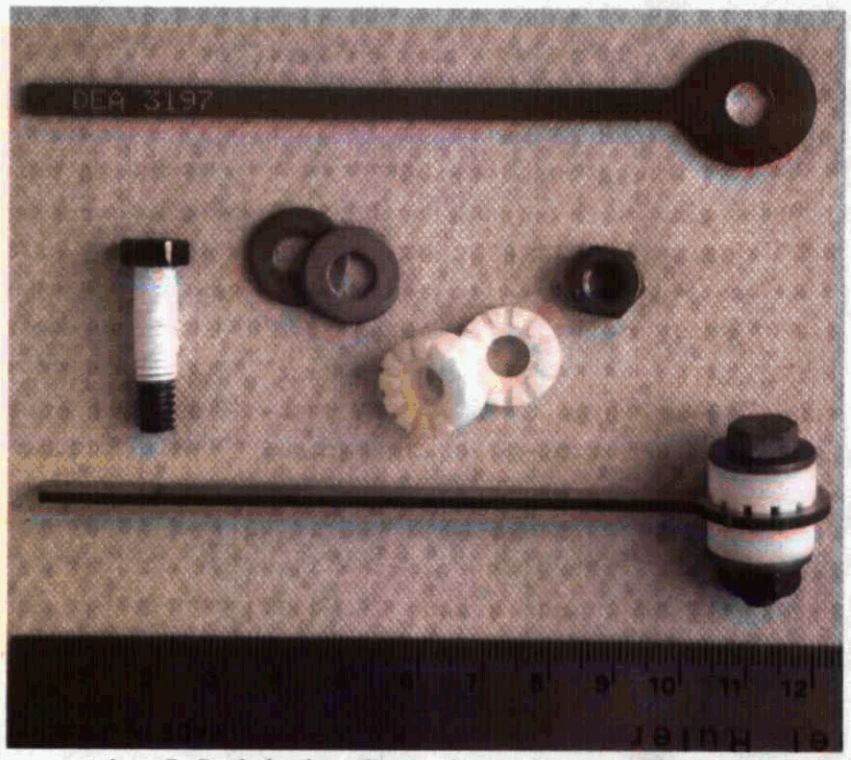

Figure 1: Multiple Crevice Assembly (MCA), bottom. It shows the lollipop-like specimen (top), titanium grade two bolt (Teflon wrapped for electrical insulation), washers nut and ceramic washers.

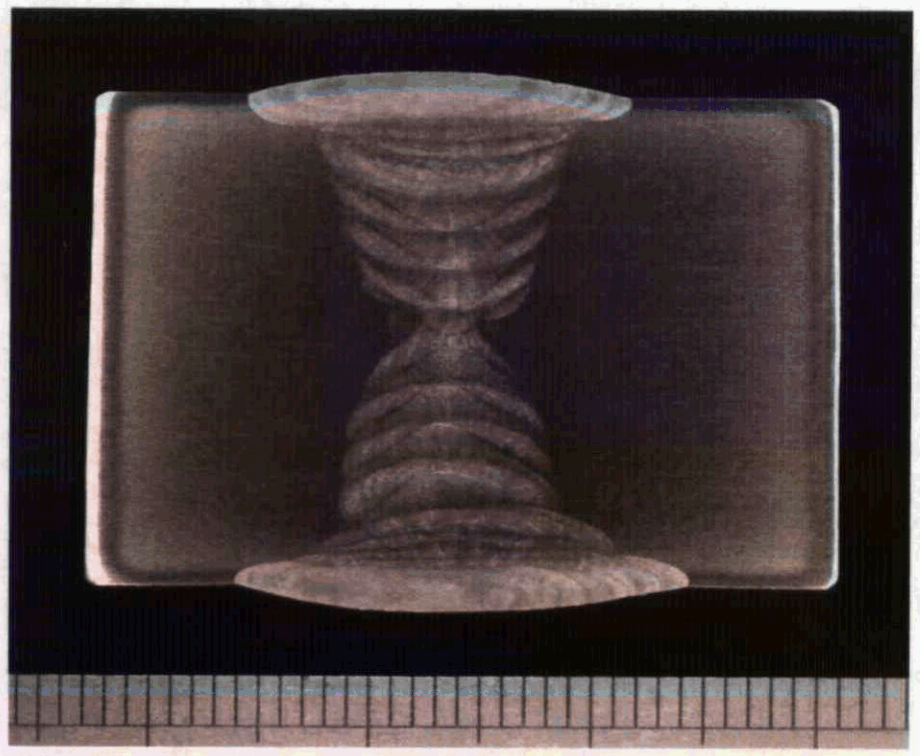

Figure 2. Cross-section of welded plate from which welded MCA samples were fabricated. Double-U weld was completed in 8-10 passes. The plate is 3.175 cm (1.25 inches) thick.

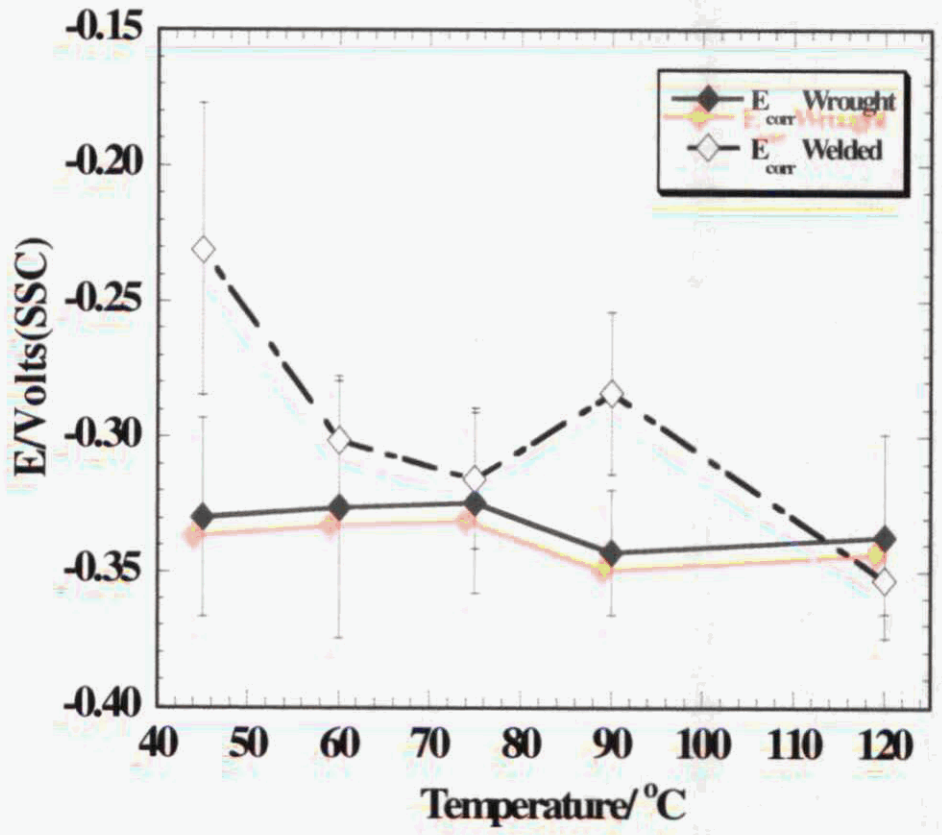


Figure 3. $E_{corr}$ as a function of temperature on wrought and welded MCA samples in 5 M $CaCl_2$. $E_{corr}$ was measured after 24 hour of immersion in solution.

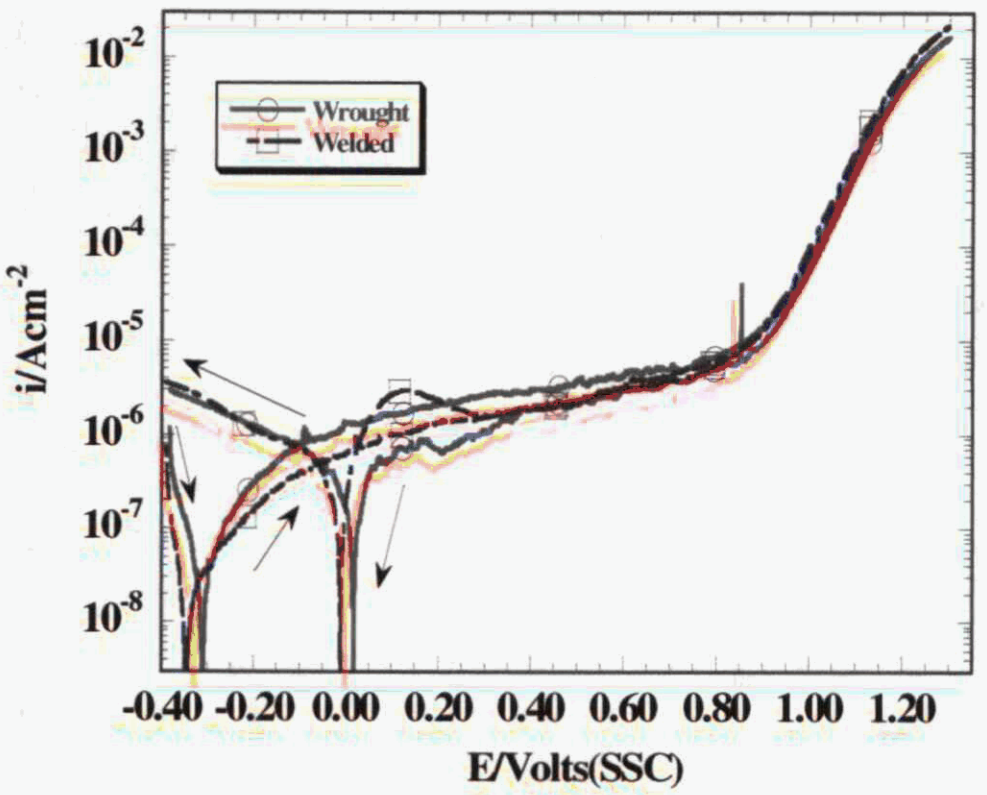


Figure 4: Polarization curves of wrought and welded MCA samples in 5 M $CaCl_2$ at 45 °C. Sweep rate, 0.1667mV/s

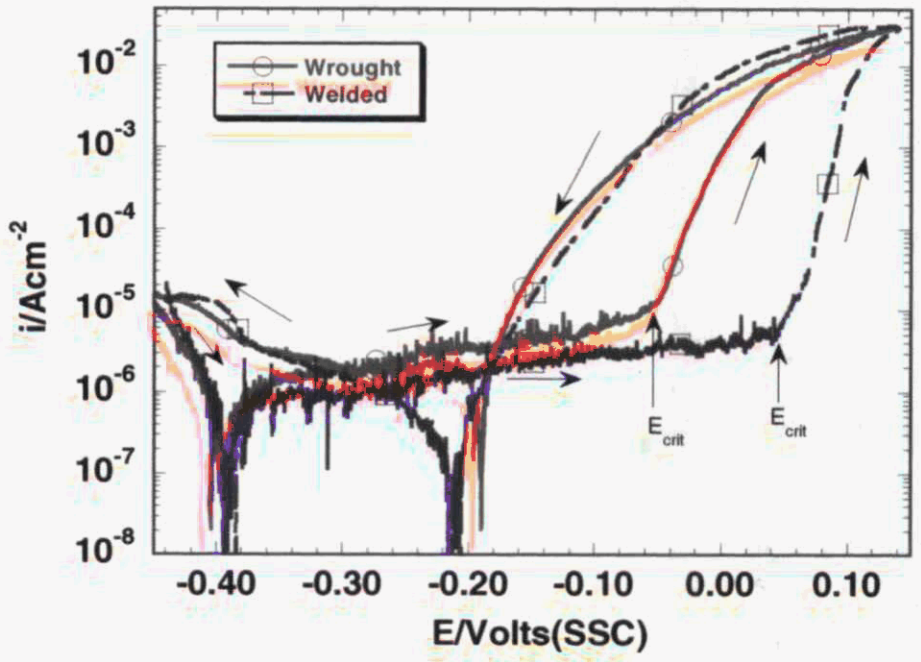


Figure 5: Polarization curves of wrought and welded MCA samples in 5 M $CaCl_2$ at 120 °C. Sweep rate, 0.1667mV/s

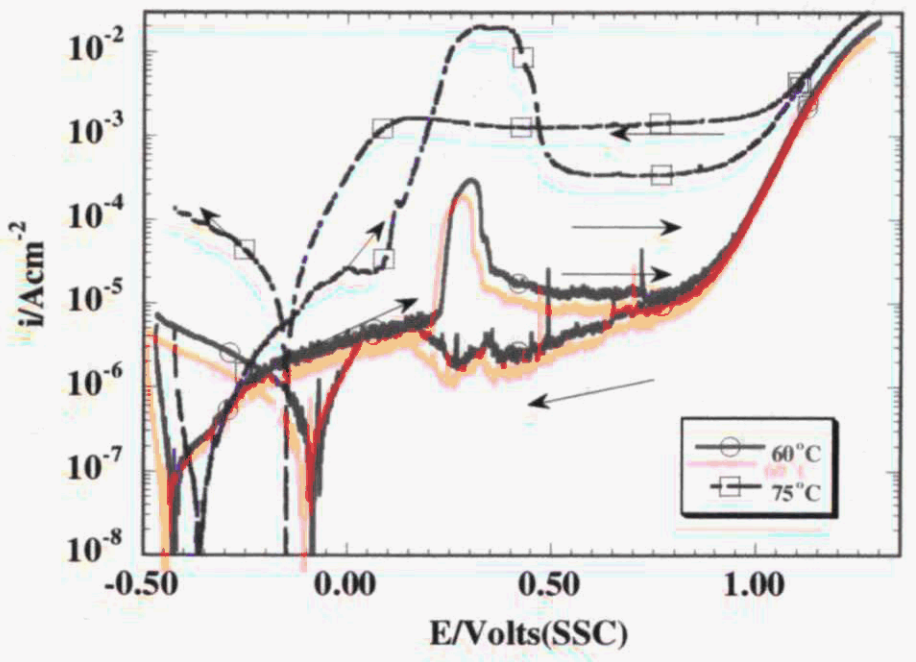


Figure 6: Polarization curves of wrought MCA samples in 5 M $CaCl_2$ at 60 and 75 °C. Sweep rate, 0.1667mV/s

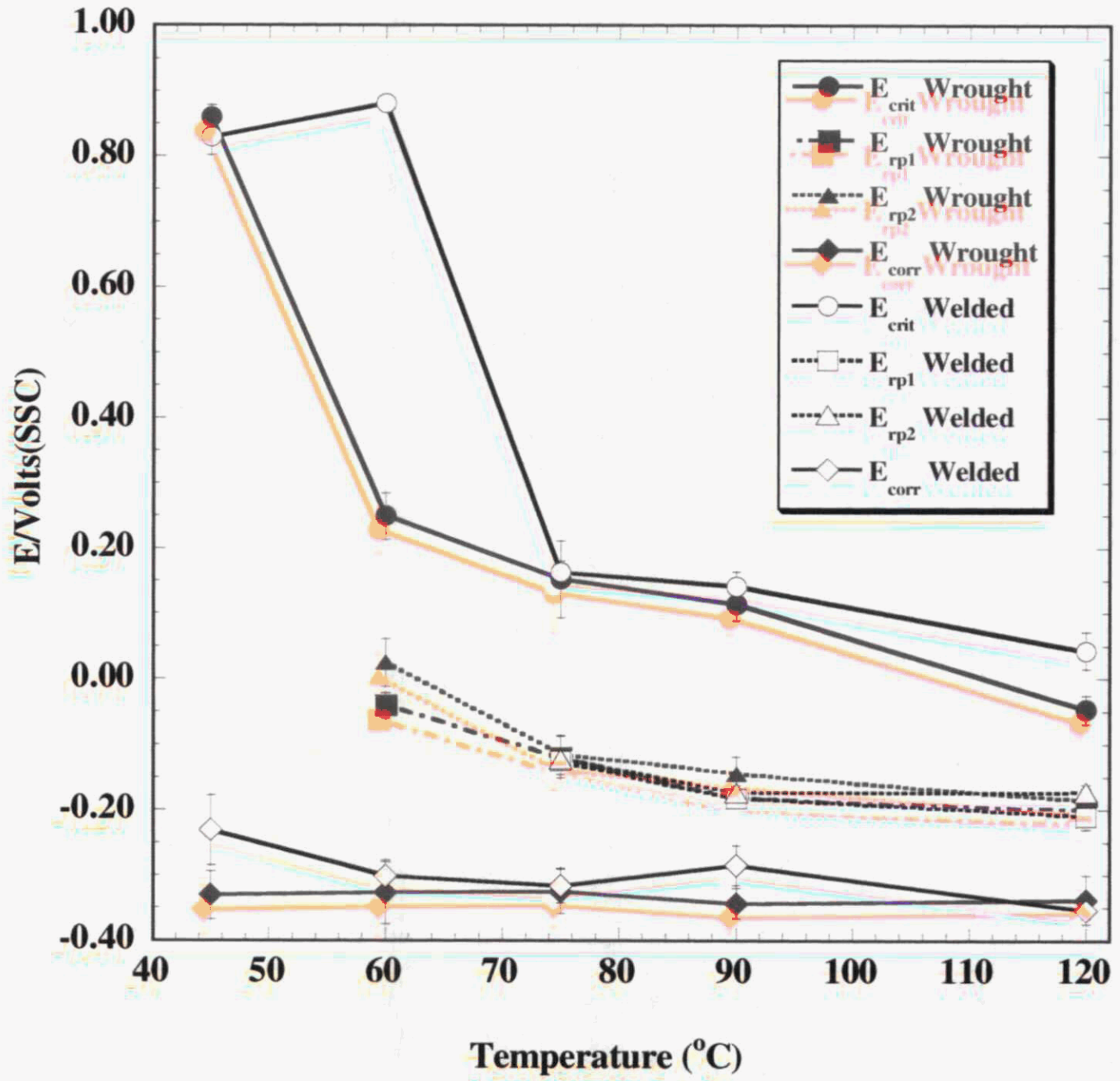


Figure 7. Average critical potential for breakdown, $E_{crit}$, the repassivation potential $E_{rp}$, and the corrosion potential $E_{corr}$, as a function of temperature on wrought and welded MCA Alloy 22 samples in 5 M $CaCl_2$. $E_{rp1}$ is the potential at which the threshold current density of 1 x $10^{-6}$ $Acm^{-2}$ was reached on the reverse sweep of the polarization curve. $E_{rp2}$ is the potential at which the reverse and forward sweeps of the polarization curve intersect.

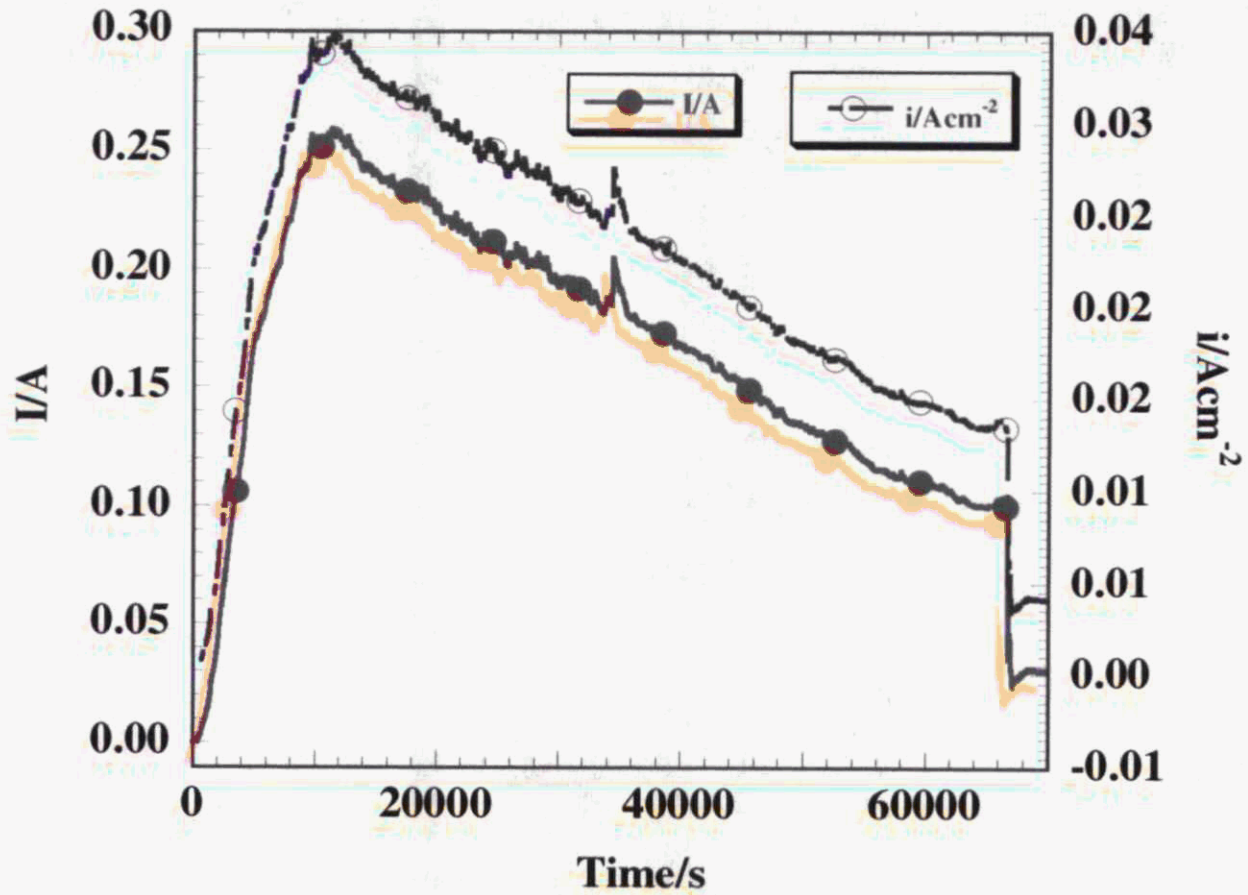


Figure 8. Current and current density transients of wrought MCA Alloy 22 at 0.325 V (SSC). These transients show 70 000s of the transient. The abrupt full in current and current density at about 67 000s possibly coincides with the detachment of the lollipop head from the stem of the sample (refer to Figure 1).

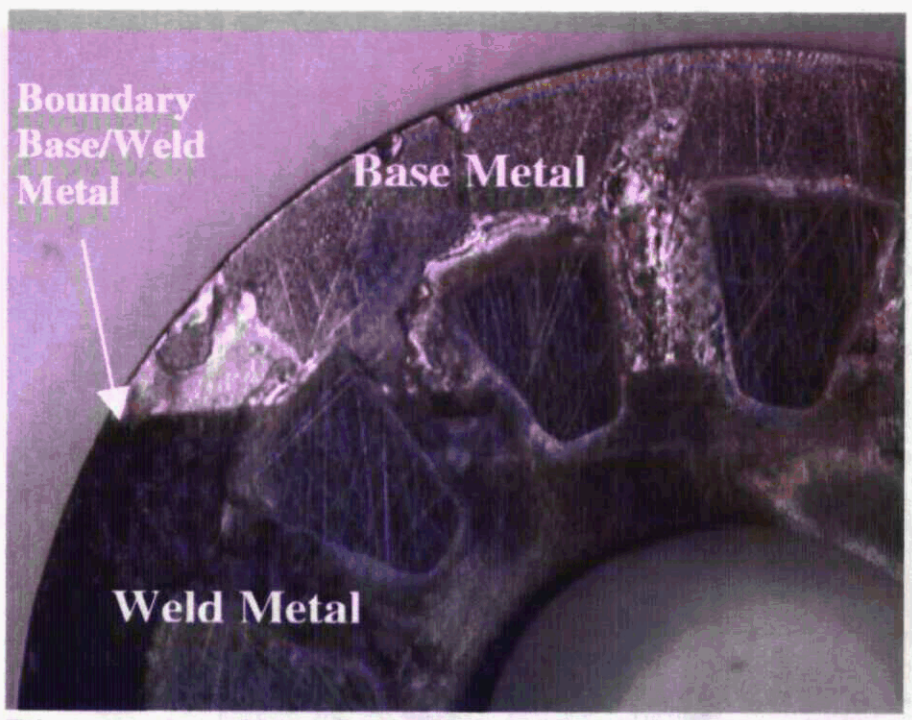


Figure 9. Welded MCA after 24 hours at $E_{corr}$, and cyclic polarization in 5 M $CaCl_2$ at 75 °C.

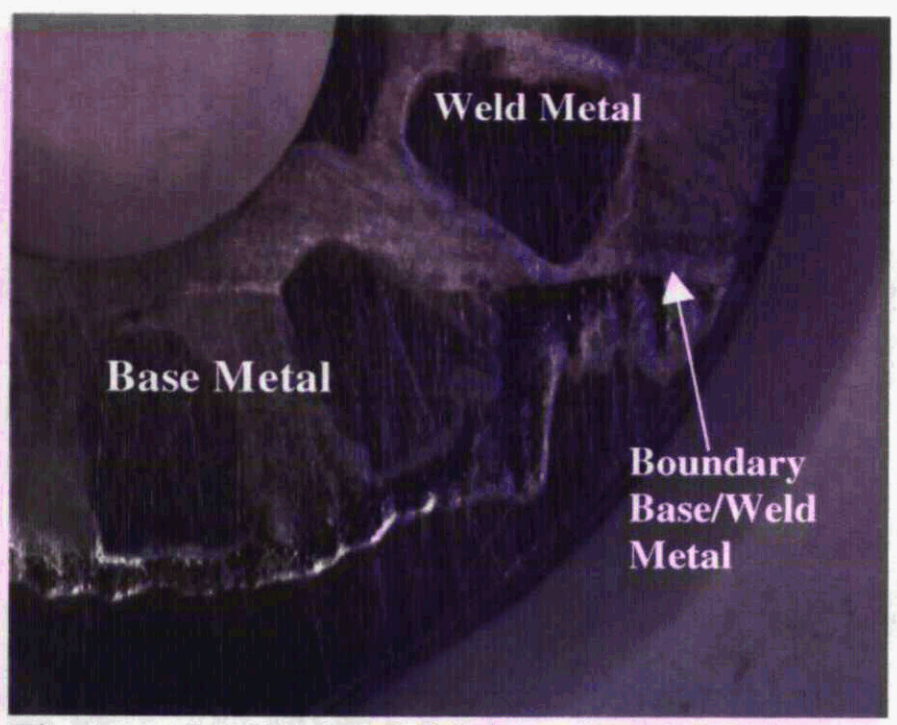


Figure 10. Welded MCA after 24 hours at $E_{corr}$, and cyclic polarization in 5 M $CaCl_2$ at 120 °C.